Modelling of blood flow resistance for an atherosclerotic artery with multiple stenoses and poststenotic dilatations

Kelvin Wong[1] Jiyuan Tu[2] Jagannath Mazumdar[3]
Derek Abbott[4]

(Received 21 February 2010; revised 3 March 2010)

Abstract

Mathematical modelling of blood flow through an artery with multiple stenoses and poststenotic dilatations is surveyed in this paper. A set of equations describes the resistance to flow ratio of an artery. Analytic solutions are based on homogenous and irrotational flow through mathematically constructed vessels. Variations in resistance to flow ratio are subjected to alterations in flow behaviour index, structural variations in relation to magnitude of vessel stenosis and multiple abnormal segments. Our analytical framework examines the effects that variability in arterial wall geometry have on the blood flow resistance. The results may aid the angiographic assessment of occlusion due to lesion development in atherosclerotic coronary arteries.

http://anziamj.austms.org.au/ojs/index.php/ANZIAMJ/article/view/2587 gives this article, © Austral. Mathematical Soc. 2010. Published March 11, 2010. ISSN 1446-8735. (Print two pages per sheet of paper.)

Contents

1 Introduction

Coronary artery disease occurs when the coronary arteries narrow to such an extent that they are unable to transport sufficient blood to the heart muscle for it to function properly. This condition is due to cholesterol plaque build-up, leading to a condition known as coronary artery atherosclerosis. The two main causes of death from coronary artery disease are rupture of the plaque causing sudden occlusion of the artery, and the slowly increasing build-up of cholesterol plaque in the artery. Angioplasty [5] reduces the risk of subsequent myocardial infarction and mitigates the long-term consequences of coronary artery stenosis.

Experimentally based models of blood flow rely exclusively on empirical data. This data is collected by invasive or non-invasive means. Angiographic machinery [6, 7, 26] assesses the reduction in flow due to these obstructions so as to provide useful physiological data for cardiologists during cardiac

diagnosis. Since the vessels are opaque to light, well established flow measurement techniques like laser Doppler velocimetry [21, 10] or particle image velocimetry [10] cannot be applied. In addition, these probes usually exceed the dimensions of fine vessels and it is difficult to attain precision in invasive blood flow experiments as probes only measure the physical properties of a fluid over a limited subset of the flow domain and their presence also alters the flow patterns.

Mathematical modelling provides an economical and non-invasive method of studying blood flow through arteries. Analytical [12, 13, 14, 16, 22] and computational [4, 11, 1] approaches can be used for arterial flow modelling. Analytical models are best suited to exploring the underlying physics of the situation and producing real time results for simpler situations. On the other hand, computational models are adept at simulating flow for complicated geometries [11, 20]. The ideal system should be as minimally invasive as possible and be able to create an accurate computational model of the vessel blood flow based on an anatomically correct geometry. An important design consideration of these patient-specific vascular modelling systems [10] is the accessibility to vascular surgeons with modest computational resources.

There is strong interest in minimally invasive operative techniques that predict the resistance to flow caused by the impingement of atherosclerotic lesions into the lumen and the subsequent extra shear stresses on the wall. Power law equations have been suggested as the physiological model of this situation. The generation of physiological data by this model, coupled with the experience of expert cardiologists, would be more helpful toward strategizing the ideal medical treatment after diagnosis.

This article examines geometrical parameters that pertain to an atherosclerotic artery with an irregular curvilinear bend and their effect on the resistance to blood flow. We assume non-Newtonian blood rheology as the basis of this analytical model. The concept of flow resistance to quantify the severity of stenosis due to atherosclerosis is not new and has been previously studied [12, 13, 14, 16]. Clinically, surgeons and physicians define the degree

of atherosclerosis by measuring percent reduction of the vessel lumen due to accumulation of atherosclerotic plaque [23, 24, 25]. However, we prove mathematically that simply measuring the plaque height is not sufficient for clinical decision making as it is not the sole parameter affecting arterial flow resistance; the proportion of the diseased segment of the atherosclerotic artery is also an important parameter.

2 Theory

2.1 Mathematical models of blood flow

Various mathematical models of blood flow in arteries have been developed and this section covers a brief formulation of the models. Forrester and Young's development of a mathematical model of blood flow in arterial vessels established an important framework in the analytical solution of non-Newtonian flow through stenosed vessels and aneurysms, elastic and viscoelastic tubes. The stenosis is constructed from the trigonometric equations for modelling [2, 3]. Solution of the approximate equations governing steady flow through stenosed arteries can be achieved [8]. Various other studies examined detailed treatment of non-Newtonian models of blood flow through rigid and elastic walled arteries [12, 13, 14, 16]. The non-Newtonian properties of blood are appropriate for the use of the Power law, Herschel–Bulkey, Casson, and Bingham models [19].

The power law or Ostwald de-Waele model describes a type of time independent non-Newtonian fluid [18, 9, 12, 22] with shear dependent viscosity. The constitutive equation of the power law model is

$$\tau = m\dot{\gamma}^n. \tag{1}$$

Here, τ is the shear stress, $\dot{\gamma}$ is the shear strain rate, m is the consistency and n is the flow behaviour index. There is no yield stress τ_0 so the equation does

not model situations where there is a finite shear stress required to overcome viscosity and start flow. The shear strain rate $\dot{\gamma}$ is a function of τ and is proportional to the rate of decrease of axial velocity v_z along the arterial radius:

$$\dot{\gamma} = f(\tau) = -\frac{dv_z}{dr}\,. \tag{2}$$

The three main categories of power law fluids are pseudo plastic, Newtonian and dilatent, which depend on the flow behaviour index. For pseudo plastic fluids, $n < 1$, the apparent viscosity decreases as the shear strain rate increases. If $n = 1$, the Power law model reduces to its Newtonian case and $m = \mu$ is the viscosity of the fluid. Bio-fluids such as blood that is described by the power law model are pseudo plastic.

2.2 Description of arterial wall geometry

The independent variables that influence the resistance to flow ratio are the characteristics of the blood, the geometry of the artery and its wall flexibility characteristics. The dimensional parameters of the typical arterial segment serve as inputs for predicting flow properties, which are important in characterizing the nature of blood flow. This section defines the geometry of the arterial wall with reference to the longitudinal plane.

Figure 1 shows the longitudinal distribution of a segment for an idealized blood vessel structure. This single lesion segment is presented from the proximal to the distal end to illustrate the case of stenosis. The axial geometry is determined by the diseased wall height D_0, shape parameter of diseased wall segment s_z for an atherosclerotic lesion of length l_0 through an artery of radius R_0. An aneurysm can be constructed by negating the value of diseased wall height D_0. Variation of s_z forms the lesion profile given by the solid, dash and dotted protrusion outlines. Here, α is the distance from the origin to the start of the diseased portion and β is the distance from the origin to the end of it. The wall equations allow both constriction (stenosis) and dilation (aneurysm) of the lumen.

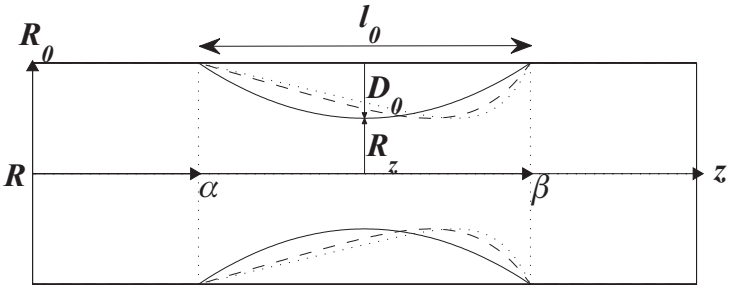

FIGURE 1: Axial variation of arterial wall with lesion development in the rz-plane.

The axial geometry $g_z(z)$ of the diseased segment is

$$g_z(z) = \begin{cases} D_0 f_z, & \text{for } \alpha \leqslant z \leqslant \beta\,, \\ 0, & \text{otherwise,} \end{cases} \tag{3}$$

and

$$f_z = f(z) = \frac{1}{l_0^{s_z}} \frac{s_z^{\,s_z/(s_z-1)}}{s_z - 1} \left[l_0^{s_z-1}(z-\alpha) - (z-\alpha)^{s_z} \right] \quad \text{for } s_z \geqslant 2\,. \tag{4}$$

Given that the normalized diseased height is

$$h_0 = \frac{D_0}{R_0} \quad \text{for } -R_0 \leqslant D_0 \leqslant R_0\,, \tag{5}$$

the equation describing the geometry of the wall after normalization is

$$\frac{R_z}{R_0} = \begin{cases} 1 - h_0 f_z\,, & \text{for } \alpha \leqslant z \leqslant \beta\,, \\ 1\,, & \text{otherwise,} \end{cases} \tag{6}$$

where s_z is a parameter determining the shape of the stenosis, and R_z is the general radius of the artery. The variation of s_z causes the shape of the stenosis or aneurysm to be skewed along the z axis. The lesion is asymmetrically profiled about the diseased centre for $s_z > 2$.

2.3 Mechanics of flow through artery with axially varying wall

Here we assume that for non-Newtonian models applied to an irrotational, anisotropic and homogeneous fluid, there is a linear relationship between the pressure and the flow, and shear independent flow with no yield stress exists. As red blood cells are 7 μm in diameter, the assumption of homogeneity would break down in narrow arteries and blood should display shear dependent flow and require a finite yield stress to be overcome before flow can commence.

The arterial flow parameters are introduced and discussed briefly. Pincombe and Mazumdar analysed axial flow through atherosclerotic arteries using numerical and analytical models [12, 13, 14, 15, 17, 16]. Dependent flow variables of interest are the reduction in flow ratio and the wall shear stress ratio. The former measures change in blood flow flux through the abnormal arterial segment. An accurate measure of reduced blood flow caused by the stenosed arteries is important for assessing the degree of atherosclerosis for patients, and indirectly assesses how much oxygen starvation the tissues supplied by the artery have experienced. Wall shear stress ratio measures the change in wall shear stress relative to the wall shear stress in a healthy artery. Assessment of this quantity is helpful to cardiologists because it is directly implicated in the genesis and development of atherosclerosis.

For variability of circumferential geometry in the transverse section of the artery, the arterial wall radius R_z is taken as a function of z. Axial velocity is denoted by v_z. The flow rate through the artery is

$$Q = 2\pi \int_0^{R_z} r v_z \, dr \,. \tag{7}$$

As presented by Pincombe and Mazumdar and using integration by parts, Q is expressed in terms of r and $\frac{dv_z}{dr}$ and by applying no-slip boundary condition, $v_z = 0$ when $r = R_z$, Equation (7) is re-expressed as

$$Q = \int_0^{R_z} r v_z \, dr = \pi \int_0^{R_z} r^2 \Big(- \frac{dv_z}{dr} \Big) \, dr \,. \tag{8}$$

Subsituting Equation (2) into (8) leads to

$$Q = \pi \int_0^{R_z} r^2 f(\tau)\, dr\,. \tag{9}$$

The shear stress

$$\tau(r) = -\frac{r}{2}\frac{dp}{dz}\,, \tag{10}$$

where p is the pressure. Therefore the value of τ at $r = R_z$ is

$$\tau_R = \tau(R_z) = -\frac{R_z}{2}\frac{dp}{dz}\,. \tag{11}$$

Re-expression of the integration in (8) and using equations (10) and (11) yields

$$Q = \frac{\pi}{\tau_R^3} {R_z}^3 \int_0^{\tau_R} \tau^2 f(\tau)\, d\tau\,. \tag{12}$$

Here, the plasma layer is assumed to be negligible and τ_R is the shear stress at the wall. With manipulation of these equations, we eventually obtain the flow resistance

$$\lambda = \frac{\Delta P}{Q} = 2m \left[\frac{(3n+1)}{n\pi} Q\right]^n \frac{1}{Q R_0^{3n+1}} I_R\,, \tag{13}$$

where

$$I_R = \int_0^{\alpha_1} dz + \sum_{i=1}^{k-1} \left(\int_{\beta_i}^{\alpha_{i+1}} dz \right) + \sum_{i=1}^{k} \left(\int_{\alpha_i}^{\beta_i} \frac{dz}{(R_z/R_0)^{3n+1}} \right) + \int_{\beta_k}^{L} dz\,, \tag{14}$$

and k is the number of diseased segments considered. Note that m is the consistency presented by the constitutive equation of the power law model, Equation (1).

The flow resistance equation takes into consideration the overlapping wall segments to form a geometrically complex shape. When comparing flow

resistance ratios, the arterial length L is arbitrarily set with a unit value of 1 to ease the mathematical formulation. For a normal artery,

$$I_N = \int_0^L dz = 1\,. \tag{15}$$

Therefore, division of flow resistance for an abnormal artery with a normal one yields the flow resistance ratio

$$\bar{\lambda} = \frac{I_R}{I_N} = I_R\,. \tag{16}$$

For a normal artery, $R_z = R_0$ and this gives a flow resistance ratio of one. For a fully occluded artery $R_z = 0$ and the flow resistance is infinite.

3 Results

3.1 Variation of flow behaviour index and wall ratio

Geometrical profiles for the arteries with a stenosis followed by an immediate aneurysm can be constructed. The generated geometrical profiles for wall ratios, $l_0/L = 1/4$, $l_0/L = 1/2$ and $l_0/L = 1$ are plotted and shown respectively in Figure 2. The curvilinear surface of $\bar{\lambda}$ can be generated for an atherosclerotic artery that has the arterial bend shape parameters, $s_z = 2$. The response maps generated by flow behaviour index, $n = 1$, $n = 2/3$ and $n = 1/3$ for an abnormal artery based on $l_0/L = 1/2$ are represented by the solid, dash and dotted meshes respectively. The maps generated for wall ratios, $l_0/L = 1/4$, $l_0/L = 1/2$ and $l_0/L = 1$ for constant flow behaviour index of $n = 1$ are represented in a similar fashion.

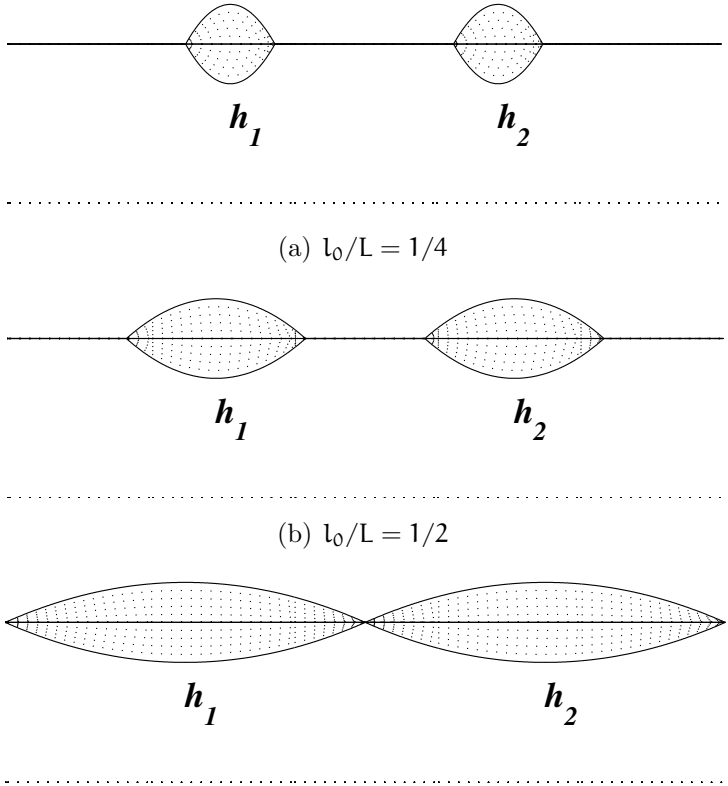

FIGURE 2: Arterial geometrical profiles for $l_0/L = [1/4, 1/2, 1]$ for non-overlapping lesions.

3.2 Flow resistance based on arterial and flow parameters

To study the effect of varying the flow and geometric properties, three surface response curvilinear maps for the flow resistance ratio are generated for different arterial configurations. Modelling of blood flow through these geometrical arteries with different flow behaviour indices and wall ratios is examined. The influence of flow behaviour based on various geometrical structuring is investigated and discussed.

The curvilinear surfaces corresponding to flow resistance ratio $\bar{\lambda}$ for the three values of flow behaviour index, $n = 1$, $n = 2/3$ and $n = 1/3$ are shown in Figure 3(a). Here, $l_0/L = 1/2$, and the diseased configuration varies from a dilation with a value of $h_0 = -0.5$ to a stenosis with a value of $h_0 = +0.5$. Therefore, the response of $\bar{\lambda}$ is based on the variable grid of (h_1, h_2) that vary from $[-0.5, -0.5]$ to $[0.5, 0.5]$. A double stenosis for the examined arterial length is shown to produce the maximum flow resistance for both plots.

The graph demonstrates that as n increases, the rate of increase in flow resistance ratio $\bar{\lambda}$ increases. The results are similar to that of the straight vessel suggested by Pincombe and Mazumdar. This signifies that the variation of stenosis and aneurysm has the same effect on flow resistance for both bend and straight vessel, and is attributed to the capillary effect of the arterial structure.

The coordinates for $\bar{\lambda} = 1$ is $(h_1, h_2) = [0.0, 0.0]$. This is also the point of inflexion based on h_1 and h_2. The surface mesh corresponding to $n = 1$ takes a greater increase in flow ratio to larger values of h_1 and h_2 from this inflexion point and a smaller reduction in $\bar{\lambda}$ for smaller values of h_1 and h_2 from the same point as compared to the mesh for $n = 2/3$ and $n = 1/3$. The variation of $\bar{\lambda}$ for $n = 1$ is less gradual as compared to the surface mesh for $n = 2/3$ and $n = 1/3$. Therefore, higher values of n are associated with more excessive values of $\bar{\lambda}$ for a given diseased height ratio. The greater difference in flow ratio between $n = 1$ and $n = 2/3$ or $n = 1/3$ indicates

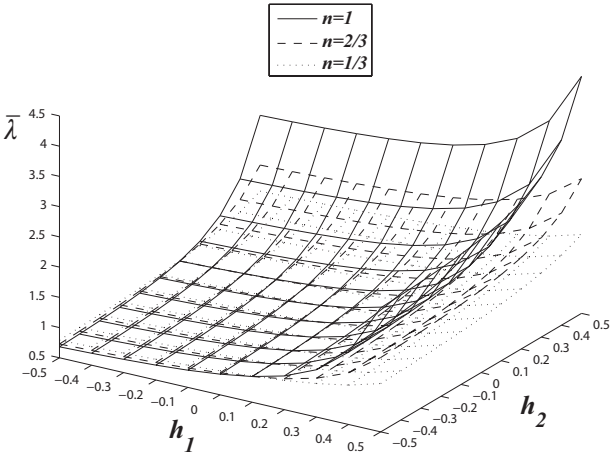

(a) Variation of flow behaviour index.

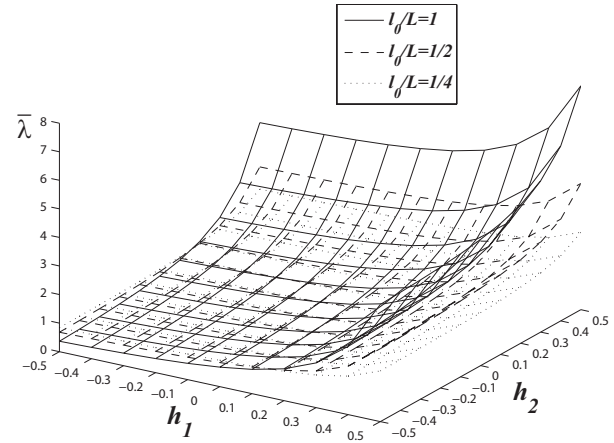

(b) Variation of wall ratio.

FIGURE 3: Flow resistance ratio $\bar{\lambda}$ surface response for three variations of (a) Flow behaviour index n and (b) Wall ratio l_0/L for an arterial configuration where $s_z = 2$.

that successive increases in n produce increasing returns.

Variations in $\bar{\lambda}$ for the three values of wall ratio, $l_0/L = [1/4, 1/2, 1]$ are shown in Figure 3(b). Successive increases in l_0/L have diminishing effects on $\bar{\lambda}$, as shown by the greater difference between the surfaces for $l_0/L = 1/4$ and $l_0/L = 1/2$ than that for $l_0/L = 1/2$ and $l_0/L = 1$. This is contrary to the variation of flow behaviour index.

Higher values of wall ratio result in an overall increasing effect in flow resistance ratio and a higher gradient of $\bar{\lambda}$ change over a (h_1, h_2) region. There is a greater separation in at specific (h_1, h_2) coordinates for a surface mesh with $l_0/L = 1$ and one with $l_0/L = 1/2$ than for a mesh with $l_0/L = 1/4$ and one with $l_0/L = 1/2$.

4 Conclusion

The ideal flow properties prediction system requires real time computation, as multiple possible intervention sites need to be investigated instantly. The type of information needed by cardiologists should be generated promptly. Mathematical modelling of atherosclerotic arteries in this research has been performed, taking into consideration the computational time, the structural modifications of the walls vis-à-vis diseased segmental ratios and wall ratio variation.

The power law model of blood flow through an atherosclerotic artery can solve the flow resistance through the abnormal segment of the artery for varying shape parameters. The variation of flow resistance pertaining to different flow behaviour indexes and wall ratios can be visualised using curvilinear surfaces projected from a two dimensional grid of values for the shape parameters. In terms of contribution to the medical field, the degree of flow resistance for arteries may serve as a guide in a clinical diagnosis.

Clinical data such as pressure drop in atherosclerotic vessels may be useful as

reference data for the assessment of flow resistance through variable arterial structures. Future studies to verify our analytical model can be performed using such clinical information.

References

[1] K. C. Ang, J. Mazumdar, and I. Hamilton Craig. A computational model for blood flow through highly curved arteries with asymmetric stenoses. *Aust. Phys. Eng. Sci. Med.*, 20(3):152–163, 1997. C68

[2] J. Forrester and D. Young. Flow through a converging diverging tube and its implications in occulsive vascular disease–i. *J. Biomech.*, 3:297–305, 1970. C69

[3] J. Forrester and D. Young. Flow through a converging diverging tube and its implications in occulsive vascular disease–ii. *J. Biomech.*, 3:307–316, 1970. C69

[4] H. W. Hoogstraten, J. G. Kootstra, B. Hillen, J. K. Krijger, and P. J. Wensing. Numerical simulation of blood flow in an artery with two successive bends. *J Biomech.*, 29(8):1075–1083, 1996. C68

[5] I. Kompatsiaris, D. Tzovaras, V. Koutkias, and M. G. Strintzis. Deformable boundary detection of stents in angiographic images. *IEEE Transactions on Medical Imaging*, 19(6):652–662, 2000. C67

[6] G. Koning, J. C. Tuinenburg, E. Hekking, J. Peelen, A. W. M. van Weert, D. Bergkamp, B. Goedhart, and J. H. C. Reiber. A novel measurement technique to assess the effects of coronary brachytheraphy in clinical trials. *IEEE Transactions on Medical Imaging*, 21(10):1254–1263, 2002. C67

[7] M. Kretowski, Y. Rolland, J. Bézy-Wendlin, and J-L. Coatrieux. Physiologically based modelling of 3-D vascular networks and CT scan

angiography. *IEEE Transactions on Medical Imaging*, 22(2):248–257, 2003. C67

[8] D. MacDonald. On steady flow through modelled vascular stenoses. *J. Biomechanics*, 12:13–20, 1979. C69

[9] J. N. Mazumdar. *Biofluid Mechanics*. World Scientific, N. J. USA, 1992. C69

[10] J. A. Moore, D. A. Steinman, S. Prakash, K. W. Johnston, and C. R. Ethier. A numerical study of blood flow patterns in anatomically realistic and simplified end-to-side anastomoses. *J. Biomech Eng*, 121:265–272, 1999. C68

[11] K. Perktolda, M. Hofera, G. Rappitscha, M. Loewa, B. D. Kubana, and M. H. Friedmana. Validated computation of physiologic flow in a realistic coronary artery branch. *J Biomech*, 31(3):217–228, 1997. C68

[12] B. Pincombe and J. N. Mazumdar. A mathematical study of blood flow through viscoelastic walled stenosed arteries. *Aust. Phys. Eng. Sci. Med.*, 18:81–88, 1995. C68, C69, C72

[13] B. Pincombe and J. N. Mazumdar. The effects of post-stenotic dilatations on the flow of a blood analogue through stenosed coronary arteries. *Mathl. Comput. Modelling*, 25:57–70, 1997. C68, C69, C72

[14] B. Pincombe and J. N. Mazumdar. Herschel–Bulkley and casson flow through viscoelastic walled stenosed arteries. *EMAC'98, The Institute of Engineers (Australia)*, E. O. Tuck & J. A. K. Stott (eds.), pages 399–402, 1998. C68, C69, C72

[15] B. Pincombe and J. N. Mazumdar. *Numerical model of power law flow through an atherosclerotic artery*, pages 563–570. CTAC'97, World Scientific Press, B. J. Noye, M. D. Teubner, 1998. C72

[16] B. Pincombe and J. N. Mazumdar. *Techniques for the study of blood flow through both constrictions and post-stenotic dilatations in arteries,*

Handbook of Computational Methods in Biomaterials, Biotechnology and Biomedical Systems. Kluwer Academic, 2002. C68, C69, C72

[17] B. Pincombe, J. N. Mazumdar, and I. Hamilton-Craig. Effects of multiple stenoses and post-stenotic dilatation on non-newtonian blood flow in small arteries. *Med. Biol. Eng. Comput.*, 37(5):595–599, 1999. C72

[18] J. Poiseuille. Observations of blood flow. *Ann. Sci. Naturelles Serie*, 5:2, 1836. C69

[19] M. C. Potter, D. C. Wiggert, and M. Hondzo. *Mechanics of Fluids*. Number 261-263. Prentice-Hall International, Inc, USA, 2nd edition, 1997. C69

[20] J. Soulis, T. Farmakis, G. Giannoglou, and G. Louridas. Wall shear stress in normal left coronary artery tree. *J. Biomech*, 39(4):742–749, 2006. C68

[21] S. C. Tjin, S. L. Ng, and K. T. Soo. In vivo Doppler shift measurements using multimode fibre optic catheters. *IEEE Transaction Biomedical Engineering*, 45:1272–1278, 1998. C68

[22] K. K. L. Wong, J. Mazumdar, B. Pincombe, S. G. Worthley, P. Sanders, and D. Abbott. Theoretical modeling of micro-scale biological phenomena in human coronary arteries. *Medical & Biological Engineering & Computing*, 44(11):971–982, 2006. doi:10.1007/s11517-006-0113-6 C68, C69

[23] S. G. Worthley, G. Helft, V. Fuster, Z. A. Fayad, J. T. Fallon, J. I. Osende, M. Roque, M. Shinnar, A. G. Zaman, O. J. Rodriguez, et al. High resolution ex vivo magnetic resonance imaging of in situ coronary and aortic atherosclerotic plaque in a porcine model. *Atherosclerosis*, 150(2):321–329, 2000. C69

[24] S. G. Worthley, G. Helft, V. Fuster, A. G. Zaman, Z. A. Fayad, J. T. Fallon, and J. J. Badimon. Serial in vivo MRI documents arterial

remodeling in experimental atherosclerosis. *Circulation*, 101(6):586–589, 2000. C69

[25] S. G. Worthley, H. M. Omar-Farouque, G. Helft, and I. T. Meredith. Coronary artery imaging in the new millennium. *Heart Lung Circ.*, 11(1):19–25, 2002. C69

[26] P. J. Yim, J. J. Cebral, R. Mullick, H. B. Marcos, and P. L. Choyke. Vessel surface reconstruction with a tubular deformable model. *IEEE Transactions on Medical Imaging*, 20(1):1411–1421, 2001. C67

Author addresses

1. **Kelvin Wong**, School of Aerospace, Mechanical & Manufacturing Engineering, RMIT University, PO Box 71, Bundoora, Victoria 3083, Australia; Centre for Biomedical Engineering and School of Electrical & Electronic Engineering, University of Adelaide, SA 5005, Australia.
mailto:k.wong@rmit.edu.au

2. **Jiyuan Tu**, School of Aerospace, Mechanical & Manufacturing Engineering, RMIT University, PO Box 71, Bundoora, Victoria 3083, Australia.
mailto:Jiyuan.Tu@rmit.edu.au

3. **Jagannath Mazumdar**, Centre for Biomedical Engineering and School of Electrical & Electronic Engineering, University of Adelaide, SA 5005, Australia.
mailto:Jagan.Mazumdar@adelaide.edu.au

4. **Derek Abbott**, Centre for Biomedical Engineering and School of Electrical & Electronic Engineering, University of Adelaide, SA 5005, Australia.
mailto:dabbott@eleceng.adelaide.edu.au